

PAPER

## Creating virtual electrodes with 2D current steering

To cite this article: Thomas C Spencer *et al* 2018 *J. Neural Eng.* **15** 035002

View the [article online](#) for updates and enhancements.

### Related content

- [Cortical activation following chronic passive implantation of a wide-field suprachoroidal retinal prosthesis](#)  
Joel Villalobos, James B Fallon, David A X Nayagam et al.
- [Visual cortex responses to suprachoroidal electrical stimulation of the retina: effects of electrode return configuration](#)  
Rosemary Cicione, Mohit N Shivdasani, James B Fallon et al.
- [Prediction of cortical responses to simultaneous electrical stimulation of the retina](#)  
Kerry J Halupka, Mohit N Shivdasani, Shaun L Cloherty et al.

# Creating virtual electrodes with 2D current steering

Thomas C Spencer<sup>1,2</sup> , James B Fallon<sup>1,2</sup>  and Mohit N Shivdasani<sup>1,2,3,4</sup> 

<sup>1</sup> Bionics Institute, East Melbourne, VIC 3002, Australia

<sup>2</sup> Department of Medical Bionics, The University of Melbourne, East Melbourne, VIC 3002, Australia

<sup>3</sup> Graduate School of Biomedical Engineering, University of New South Wales, Kensington, NSW 2033, Australia

E-mail: [m.shivdasani@unsw.edu.au](mailto:m.shivdasani@unsw.edu.au)

Received 7 November 2017, revised 3 February 2018

Accepted for publication 23 February 2018

Published 28 March 2018



## Abstract

**Objective.** Current steering techniques have shown promise in retinal prostheses as a way to increase the number of distinct percepts elicitable without increasing the number of implanted electrodes. Previously, it has been shown that ‘virtual’ electrodes can be created between simultaneously stimulated electrode pairs, producing unique cortical response patterns. This study investigated whether virtual electrodes could be created using 2D current steering, and whether these virtual electrodes can produce cortical responses with predictable spatial characteristics.

**Approach.** Normally-sighted eyes of seven adult anaesthetised cats were implanted with a 42-channel electrode array in the suprachoroidal space and multi-unit neural activity was recorded from the visual cortex. Stimuli were delivered to individual physical electrodes, or electrodes grouped into triangular, rectangular, and hexagonal arrangements. Varying proportions of charge were applied to each electrode in a group to ‘steer’ current and create virtual electrodes. The centroids of cortical responses to stimulation of virtual electrodes were compared to those evoked by stimulation of single physical electrodes. **Main results.** Responses to stimulation of groups of up to six electrodes with equal ratios of charge on each electrode resulted in cortical activation patterns that were similar to those elicited by the central physical electrode (centroids: RM ANOVA on ranks,  $p > 0.05$ ; neural spread: one-way ANOVA on Ranks,  $p > 0.05$ ). We were also able to steer the centroid of activation towards the direction of any of the electrodes of the group by applying a greater charge to that electrode, but the movement in the centroid was not found to be significant. **Significance.** The results suggest that current steering is possible in two dimensions between up to at least six electrodes, indicating it may be possible to increase the number of percepts in patients without increasing the number of physical electrodes. Being able to reproduce spatial characteristics of responses to individual physical electrodes suggests that this technique could also be used to compensate for faulty electrodes.

**Keywords:** current steering, retinal prosthesis, electrical stimulation, retina, visual cortex, retinitis pigmentosa, virtual electrodes

(Some figures may appear in colour only in the online journal)

## Introduction

Retinal prostheses are currently the only approved treatment for retinitis pigmentosa, a group of hereditary degenerative retinal diseases that affect over one million people worldwide [1–3].

These devices provide artificial vision to patients by electrically stimulating surviving non-photosensitive neurons in the inner retinal layers. Electrical stimulation of the retina elicits the perception of discrete flashes of light [4, 5]. These percepts, termed phosphenes, are used as building blocks to construct an artificial image, much like pixels on a computer monitor [1, 2]. Clinical studies have shown that retinal prostheses can improve

<sup>4</sup> Author to whom any correspondence should be addressed.

patient performance in spatio-motor tasks, pattern recognition, and basic object recognition [6–8]. However, due to the poor visual acuity afforded by present-generation devices, more complex tasks such as independent navigation, facial recognition, and reading, barring in a few exceptional patients, are still out of reach. Technical and safety constraints limit the size and density of electrode arrays which, using conventional single electrode stimulation techniques, directly limits the range of percepts that can be elicited.

Current steering refers to a number of stimulation techniques aimed at manipulating the distribution of electrical potential around electrode sites [9–11]. These techniques make use of simultaneous stimulation of electrodes in a controllable fashion to shift the peak of the summated electrical field, in order to target specific neural populations. Interactions between electrical fields are often considered to be undesirable, as they can result in unpredictable temporal or spatial smearing of the percept [12–14], so they are typically circumvented using sequential stimulation presented within the flicker fusion rate of the visual system. However, this limits the number of phosphenes to the number of implanted electrodes, which is in turn subject to engineering and surgical constraints. Incorporating electrical field interactions into the stimulation strategy may allow an increase in the number of unique percepts without significant changes to the electrode array.

The perceptual effects of electrical field interactions between simultaneously stimulated electrodes has been explored in cochlear implants. So called ‘virtual’ electrodes can be created between simultaneously stimulated adjacent electrode pairs, eliciting the perception of an intermediate pitch [15–17]. This technique is implemented clinically to increase the auditory spectral resolution afforded to patients [16, 17]. Current steering in deep brain stimulation between up to four linearly arranged electrodes has also been shown to mitigate dyskinesia side effects in Parkinson’s patients, presumably by shifting the peak of the summated electrical field away from undesired neural populations [18, 19]. In the retina there have been a number of pre-clinical studies into the effects of field shaping techniques. Virtual electrodes can be created between two physical electrode pairs [10]. Increasing the proportion of charge delivered to one of these electrodes can also shift the virtual electrode towards it [10]. Interactions between many simultaneously stimulated retinal electrodes can also be used to reduce current spread, thereby reducing the spread of neural activation [20], and have been shown to be capable of modulating the firing probability of individual retinal ganglion cells [21]. Cortical responses to simultaneous stimulation of up to 42 electrodes can also be predicted by constructing a model from cortical responses to white-patterned stimuli [22], demonstrating that neural responses to simultaneous multichannel stimulation are repeatable and consistent. Current steering therefore shows significant promise in increasing the range of percepts that can be presented to patients. However, it is unclear whether these techniques are likely to provide percepts that are useful in presenting complex visual information to patients. The relationship between cortical activity elicited by physical and virtual electrode stimulation has not been extensively studied,

and accurate prediction of responses depends on extensive sampling of cortical activity [22].

This study aims to further investigate the creation of virtual electrodes using 2D current steering. In this study we specifically aimed to determine whether we could reproduce the properties of cortical responses to physical electrodes, by steering current between differing numbers of adjacent electrodes. Electrode failure is a significant issue for prosthetic devices and is a major factor in efficacy and lifespan [23, 24]. Virtual electrodes have the potential to mitigate this issue by replacing faulty physical electrodes, reducing the functional deficits of reduced phosphene counts and the potential damage associated with repeated repair and reimplantation. We also aimed to confirm that the ability to shift virtual electrodes by altering the proportions of charge is maintained when using different 2D electrode arrangements, and to determine whether the spatial properties of the resultant cortical response could be predicted based only on the knowledge of stimulation weights applied.

## Methods

### *Anaesthesia and surgery*

All procedures were approved by the Bionics Institute Animal Research Ethics Committee (Project #14 304AB) and were in accordance with the Australian Code of Practice for the Care Use of Animals for Scientific Purposes (8th edition) and with the National Institute of Health, USA guidelines regarding the care and use of animals for experimental procedures. Normally sighted adult cats ( $n = 7$ ) were used in this study. Due to increased regulation of the supply of pentobarbital in Australia, two different anaesthetic protocols were followed. Five of the seven cats were sedated with ketamine (intramuscular [i.m.], 20 mg kg<sup>-1</sup>) and xylazil (subcutaneous [s.c.], 2 mg kg<sup>-1</sup>). Anaesthesia was maintained over the experimental period for up to 3 d with a continuous intravenous (i.v.) infusion of sodium pentobarbitone (3–8 mg/kg/h) as per our previous studies [5, 20, 25]. A continuous i.v. infusion of Hartmann’s solution (sodium lactate, 2.5 ml/kg/h) was also administered throughout the experiment. The remaining two cats were sedated with ketamine (i.m. 8 mg kg<sup>-1</sup>), medetomidine (i.m. 0.012 mg kg<sup>-1</sup>), and methadone (i.m. 0.4 mg kg<sup>-1</sup>). Anaesthesia was maintained with continuous i.v. infusion of propofol (24 mg kg<sup>-1</sup>). A continuous i.v. infusion of methadone in Hartmann’s solution (0.25 ml of 10 mg ml<sup>-1</sup> methadone in 250 ml compound sodium lactate, 0.05 mg/kg/h) was also administered throughout the period of anaesthesia. Due to the depressive effects of propofol on the respiratory system, tracheostomies were performed and the animals ventilated on 100% oxygen (20–25 breaths min<sup>-1</sup>) (model 6025; Ugo Basile, Monvalle, VA, Italy). Respiration rate, heart rate, end-tidal CO<sub>2</sub>, blood pressure and temperature were monitored consistently throughout the experiment and maintained at normal levels by adjusting the anaesthetic flow rate. Daily injections of dexamethasone (i.m. 0.1 mg kg<sup>-1</sup>) and clavulox (s.c. 10 mg kg<sup>-1</sup>) were administered to all seven cats. Pupils were dilated by regular topical application of a mixture of phenylephrine hydrochloride (2.5%) and tropicamide (1%).

The suprachoroidal electrode array was similar to that which has been used in our previous work [6, 26], fabricated on a biocompatible silicon substrate and consisting of 42 platinum electrodes of 600  $\mu\text{m}$  diameter spaced 1 mm from centre to centre. The implantation procedure is detailed in our previous studies [26, 27]. Briefly, following a lateral canthotomy, scleral incision, and dissection of a pocket between the sclera and choroid, the array was inserted ~15 mm into the suprachoroidal space until the tip was beneath area centralis. Our aim during implantation is to encompass as much of the area centralis as possible. The array is typically placed over the area centralis, often relatively superior and temporal in order to avoid contact with the optic disc. Electrical connections to the electrodes on the array were tested using an automated impedance monitoring software developed in LabVIEW (National Instruments, Austin, TX, USA) used in previous studies [28]. The animal was placed in a stereotaxic frame inside a darkened electrically shielded room. Visual inspection of the eye and fundus photographs were taken to determine the health of the eye and positioning of the array. A craniotomy was then performed spanning 15 mm rostral and 5 mm caudal from the interaural line, and 7 mm lateral from the sagittal suture on the side contralateral to the implanted eye, exposing the visual cortex. A number of studies have shown that, in normally sighted cats, most cells located nasally relative to the area centralis project to the contralateral hemisphere. Additionally, some temporally located cells, particularly those close to the area centralis, also project to the contralateral hemisphere [29–32]. The dura mater was carefully excised from the region. Using two parylene-based flexible platinum electrode arrays (as described in Fallon *et al* 2016 [33]), electrically evoked potentials (EPs) in response to cathodic-leading biphasic charge-balanced current pulses (0–750  $\mu\text{A}$ , 1 ms per phase) were mapped along the surface of the visual cortex to determine the cortical region with the lowest EP thresholds. Up to two planar ‘Utah’ 36- ( $6 \times 6$ ) or 60- ( $6 \times 10$ ) channel penetrating microelectrode arrays (Blackrock Microsystems, Foxborough, MA, USA) were inserted in the regions of Area 17/18 of the visual cortex with the lowest EP thresholds to a depth of approximately 1 mm. The recording electrodes were separated by a distance of 400  $\mu\text{m}$  and sampled ~7.2 mm<sup>2</sup> and ~4 mm<sup>2</sup> of the cortex for the 60- and 36- channel arrays respectively. Recording electrodes are 1 mm in length with a pitch of 400  $\mu\text{m}$ . Based on manufacturer estimates, the exposed platinum tip of each electrode is 50  $\mu\text{m}$  long and, at its thickest point,  $23 \pm 12$   $\mu\text{m}$  in diameter. Assuming a uniformly conical tip shape, this translates to an approximate surface area ranging from 2.15 mm<sup>2</sup> to 10.56 mm<sup>2</sup>. The size and number of electrode arrays used for each animal was determined by the prevalence and location of large blood vessels, as care was taken to minimise damage these structures during insertion.

### Experimental protocols

Electrical stimuli were generated with a 128-channel IZ2 stimulator (Tucker-Davis Technologies, Alachua, FL, USA). Due to the low maximum current output per channel (300  $\mu\text{A}$ ),

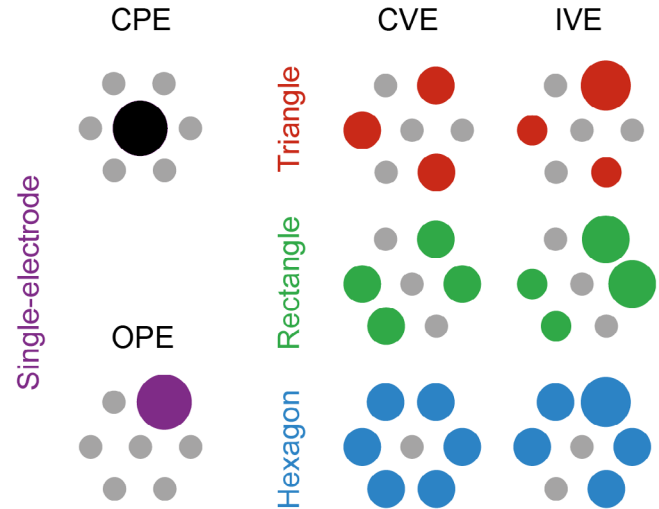


**Figure 1.** Diagram showing the different combinations of electrode shapes and stimulation configurations. Grey circles represent unstimulated electrodes on the stimulating array. Larger circles in other colours represent electrodes being stimulated. The size of the electrodes shows the proportion of charge delivered (not to scale). CPE stimulation is where the central electrode of the shape is stimulated, and OPE stimulation is where an outer electrode of the shape is stimulated. Central virtual electrode (CVE) stimulation is where charge is distributed evenly between the OPEs. IVE stimulation is where charge is unevenly distributed amongst the OPEs, with the aim of creating a virtual electrode between the CPE and the OPE with the greater proportion of the charge. Note that the total charge delivered when using all stimulation modes was kept the same.

each group of three channels was combined using a custom-built circuit board bringing the maximum functional number of combined stimulating channels to 42 and the maximum current output to 900  $\mu\text{A}$  per combined channel. Each combined channel was connected directly to an electrode on the suprachoroidal array enabling independent simultaneous stimulation of all 42 electrodes. Pulses were presented at randomly varied currents ranging from zero to 750  $\mu\text{A}$  in 50  $\mu\text{A}$  steps at a repetition rate of 1 Hz. Each current step was repeated ten times. Stimulus pulses were cathodic-first and symmetrically biphasic with a 1000  $\mu\text{s}$  phase width and 25  $\mu\text{s}$  interphase gap. Either all the charge from each pulse was presented to a single electrode or the total charge was split across groups of electrodes for steered stimulation according to predefined charge ratios. Thus the maximum charge delivered to the retina was capped to 750 nC corresponding to a maximum charge density of 265  $\mu\text{C cm}^{-2}$  (for single electrode stimulation), which is below the safe limit for gassing when using platinum electrodes [34]. Platinum needle electrodes were placed in the conjunctiva to provide an extraocular return path.

Stimulating electrode groups were chosen in three predefined geometric shapes: triangles, rectangles, and hexagons (shown in figure 1). For each arrangement, it was important that the electrode groups contained a single electrode in its centre that was not part of the group but stimulated on its own as we wanted to assess if a similar cortical response could be obtained between single and steered multi-electrode stimulation. Four stimulus configurations were used for each shape: central physical electrode (CPE) stimulation, whereby the

single electrode in the centre of the shape received all the charge. Central virtual electrode (CVE) stimulation, whereby the outer electrodes of the shape received equal proportions of charge, with the intention of creating a virtual electrode in the same area as the CPE. Intermediate virtual electrode (IVE) stimulation, where certain electrodes received a greater proportion of charge, depending on the geometric shape. For triangular electrode shapes, half the charge was delivered to one electrode, while the other two electrodes each received one quarter of the charge. For rectangular electrode shapes, two electrodes received one third of the charge each, while the others each received one sixth. For hexagonal electrode shapes, only five of the six electrodes received charge with one third of the charge applied to one outer electrode, no charge delivered to the electrode opposite, and the other four electrodes each receiving one sixth. Due to experimental time constraints other charge ratios were not explored. IVE stimulation was repeated for each electrode shape, while rotating the outer electrodes that received proportionally greater charge. Finally, outer physical electrode (OPE) stimulation was also performed where an outer electrode received all the charge. This was done as a control to confirm that responses were different between different single electrodes. OPE stimulation was also repeated for each outer electrode in each shape.

#### Data analysis

Cortical recordings were analysed using custom scripts written in Igor Pro (Wavemetrics, Lake Oswego, OR, USA) and Matlab (Mathworks, Natick, MA, USA). Signal artefacts were removed using techniques described by Heffer and Fallon [35]. The signal was bandpass filtered after artefact removal (Butterworth filter 0.3–5 kHz; order 3) and spikes were timestamped when the signal exceeded four times the root mean square value. Spikes detected within a 3–20 ms window were included in the analysis, as it is hypothesised to corresponding to both direct activation of retinal ganglion cells and indirect activation of the network [36], and to remain consistent with earlier studies [10, 20, 37–39]. For each recording, the number of spikes were counted 3–20 ms prior to the stimulus in order to estimate the spontaneous firing rate. The average spontaneous firing rate over the ten stimulus repeats was subtracted from spike rates recorded during the evoked response period. For each recording channel, spike rates averaged across the ten repetitions of each current step were used to construct an input–output function and a sigmoid curve was fitted. Consistent with our earlier studies [39, 40], threshold was defined as the level of charge where the sigmoid curve reached 50% of the maximum saturated spike rate on the recording channel. For each stimulus configuration, the recording channel with the lowest threshold was designated the best cortical electrode (BCE). Cortical spatial maps were constructed by plotting the spike rate across all recording channels at the threshold charge of the BCE, normalised to the maximum spike rate on each recording channel.

To characterise the spatial characteristics of cortical responses, we calculated the weighted centroid and neural activation spread of the cortical spatial maps. Centroids were

calculated as a normalised spike-rate weighted centre of mass across all channels, according to the following formula:

$$\bar{x} = \frac{\sum_{i=1}^n m_i x_i}{\sum_{i=1}^n m_i}$$

$$\bar{y} = \frac{\sum_{i=1}^n m_i y_i}{\sum_{i=1}^n m_i}.$$

Where  $(\bar{x}, \bar{y})$  are the coordinates of the centroid and  $m_i$  is the normalised spike rate from each electrode site (i.e.  $m_1, m_2, \dots, m_n$ ) and  $x_i$  and  $y_i$  are the coordinates of each electrode site (i.e.  $(x_1, y_1), (x_2, y_2), \dots, (x_n, y_n)$ ).

Applying the same stimulation to the retina typically results in similar, but not identical, cortical responses. This can be due to a number of factors, such as changes to impedance in the choroid due to inflammation, sensitisation to previous stimuli, depth of anaesthesia, or central neural influences. As such, cortical responses to two different sets of CPE stimulation were recorded, in order to determine the average degree of inherent variation in centroid position to identical stimulation. Centroids calculated for the repeat of CPE stimulation, as well as for CVE, IVE and OPE stimulation were compared in distance from the centroid calculated for the original CPE stimulation run. As there were multiple iterations of IVE and OPE stimulation for each electrode shape, the distances for each stimulation mode were averaged for each shape. The average shift in cortical centroid for each of the stimulation configurations compared to the original CPE run were compared with a repeated measures ANOVA. We hypothesised that the average centroid shift between responses elicited by CPE and CVE stimulation should not be greater than the shift calculated between repeats of CPE stimulation. Ideally, IVE stimulation should create a virtual electrode between the central and OPEs, as such we expected the average centroid shift between responses to CPE and IVE stimulation to be greater than repeats of CPE stimulation, but less than the shift calculated between CPE and OPE stimulation.

The spread of neural activation was calculated for each configuration using the method described by Cicione *et al* [39]. Normalised spike rates on each channel at the charge required to reach 90% of the maximum saturating spike rate on the BCE were plotted as a function of distance from the BCE. A decaying exponential was fitted and the inverse tau used to quantify cortical selectivity. Activation spread was measured for each stimulus configuration of each electrode shape. Our previous work showed no significant difference in the activation spread of responses elicited by physical electrodes and virtual electrodes created by stimulation of electrode pairs [10]. We expected this to be maintained in virtual electrodes created by 2D electrode shapes.

In addition to measuring centroid shift, we also devised a method to predict the expected direction of centroid shift based on work done by Tusa *et al* on the retinotopic mapping in Brodmann areas 17 [41] and 18 [42]. We predicted that superior movement of the peak of the electrical field in the retina would translate to rostral movement in the centroid of contralateral cortical activation, and that temporal movement in the retina would translate to lateral movement in the



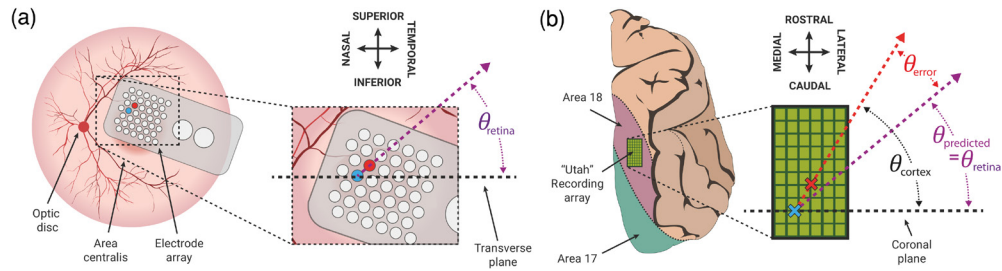


**Figure 2.** Diagram illustrating our method of predicting the direction of centroid shift. (a) shows the method of deriving  $\theta_{retina}$ . The blue electrode represents the electrode at the centre of an electrode shape, and the red electrode represents an outer electrode of a shape, which is either being stimulated independently, or has received the greatest proportion of charge as part of IVE stimulation. The angle between these two electrodes relative to the transverse plane of the eye is  $\theta_{retina}$ . (b) shows the method of deriving  $\theta_{prediction}$  from  $\theta_{retina}$ . The blue and red crosses represent the location of the centroid of the responses elicited by stimulation of the blue and red electrodes from (a). The purple dotted line represents  $\theta_{prediction}$ , which equals  $\theta_{retina}$ , relative to the coronal plane of the cortex. The red dotted line represents  $\theta_{cortex}$ , which is the measured angle between the centroids. The difference between  $\theta_{prediction}$  and  $\theta_{cortex}$  is designated  $\theta_{error}$ .

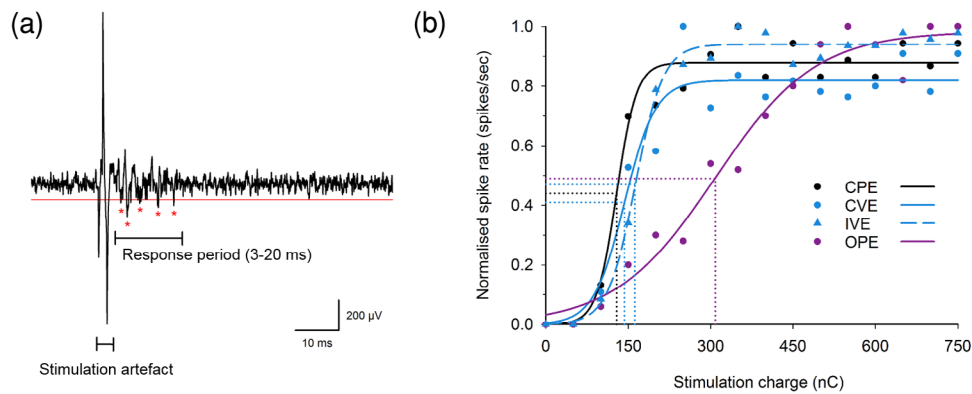


**Figure 3.** Examples of electrically evoked multiunit activity on a single cortical recording channel. (a) Recording of multiunit activity on a single recording channel in response to stimulation of a single retinal electrode. Stimulation artefact and the recorded response are highlighted. The red line denotes the  $-3$  RMS threshold, and asterisks denote detected spikes. (b) Input-output functions of a single cortical channel in response to CPE (black circles), CVE (blue circles), IVE (blue triangles), and OPE (purple) stimulation of the same hexagonal electrode shape. Dots represent the average normalised spike rate at each discrete charge interval. The solid and dashed lines show the sigmoid fit for each dataset. The dotted lines show the point of the sigmoid that corresponds to the threshold (50% of saturating spike rate) (CPE: 128.8 nC, CVE: 143 nC, IVE: 158 nC, OPE: 308.5 nC). Note the similarity between the threshold and sigmoid fit characteristics between CPE, CVE and IVE stimulation. As the peak of the electrical field shifted to an adjacent electrode when performing OPE stimulation, the threshold for this cortical channel increased.

cortical centroid. The location of each physical electrode in the eye was determined from fundus images taken post-implantation. Using this translational mapping technique, we attempted to predict the direction of the cortical centroid shift based on angles measured in the retina between physical electrodes, and the expected position of virtual electrodes. We expected that the angle between the peaks of the electrical field in the retina ( $\theta_{retina}$ ), relative to the transverse plane of the eye, would be similar to the angle between the centroids of the resultant cortical responses ( $\theta_{cortex}$ ), relative to the coronal plane of the brain (illustrated in figure 2). To validate our technique, we first attempted to predict the angle of centroid shift between CPE and OPE stimulation, as the locations of physical electrodes are known in the retina. Assuming the peak of the electrical field in the retina is centred at the same location as the stimulated electrodes, we measured the angle between the electrodes from the fundus images. This angle was rotated in accordance with the directional mapping between retina and cortex explained above to give a predicted angle of centroid shift ( $\theta_{predicted}$ ). The actual angle between the two centroids elicited was then measured. The difference

( $\theta_{error}$ ) between  $\theta_{predicted}$  and  $\theta_{cortex}$  were plotted in a polar frequency histogram and placed in bins with a  $45^\circ$  width. Rayleigh's test was used to measure uniformity of the circular distribution and, if shown to be non-uniform, a circular mean was calculated. We expected that  $\theta_{error}$  values will not be uniformly distributed, and would have a near-zero circular mean if the centroids moved in the same direction as we expected them to. Following successful validation of our technique, we attempted to predict the direction of centroid shift between CVE stimulation and IVE stimulation, assuming that CVE stimulation would produce an electrical field with a peak over the CPE, and that IVE stimulation would result in a centroid shift in the direction of the electrode or electrodes with the greatest proportion of charge.

## Results

### Differences between anaesthetic protocols

No significant difference was found in the latency or maximum firing rate of electrically-evoked cortical responses between

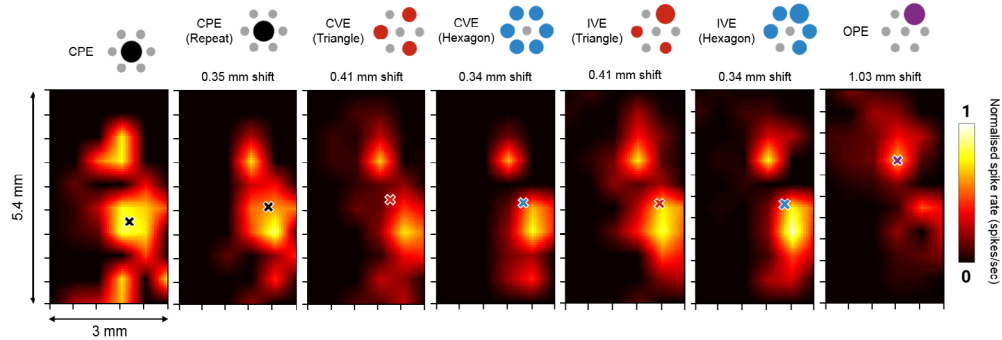


**Figure 4.** Examples of cortical spatial maps constructed in response to the different stimulation configurations. Smoothing has been applied to the maps using linear interpolation of the values at neighbouring grid points in each direction. Recording electrodes lie on the intersections of the axes ticks. For this example, the triangular and hexagonal electrode shapes share the same CPE and OPEs. Weighted centroids are marked on each spatial map by an X. Note the similarities in centroid locations and activation patterns between the virtual electrodes and the CPE repeats but a significant shift in the centroid when one of the OPEs was stimulated. The shift of the centroids from the centroid calculated for the first run of CPE stimulation is labelled above each map.

the two different anaesthetic protocols ( $p$ 's  $> 0.05$ , Mann-Whitney U test). However, there was a statistically significant increase in spontaneous firing rates, rising from an average of  $2.18 \text{ spikes s}^{-1}$  ( $n = 39563$  cortical channels) in cats anaesthetised with pentobarbital to  $3.07 \text{ spikes s}^{-1}$  ( $n = 8940$  cortical channels) in cats anaesthetised with a combination of propofol and methadone ( $p < 0.001$ , Mann-Whitney U test). While statistically significant, we do not believe that the rise in spontaneous firing rate between the groups is of a sufficient magnitude to affect our spike analysis methods given we subtracted spontaneous firing from the spike count obtained in the 3–20 ms window. Given these results, the data collected from all animals were combined and analysed in the same fashion regardless of anaesthetic protocol.

#### Reproducing responses to physical electrodes with virtual electrodes

For this analysis, shapes were only included if a threshold could be calculated from at least one recording channel in response to two repeats of CPE stimulation, and at least one run of CVE, IVE and OPE stimulation. Cortical responses were collected from 38 triangular and 19 hexagonal shapes with all modes of stimulation applied, totalling 342 physical electrodes. Unfortunately, two sets of CPE stimulation were not recorded for rectangular shapes due to time constraints and technical issues, and as such are excluded from this analysis. Examples of IO plots for each stimulus mode of a hexagonal electrode shape are shown in figure 3. Using these criteria, 18 triangular and eight hexagonal shapes were included in this analysis. No significant differences in lowest cortical thresholds were found between stimulation of single physical electrodes (i.e. CPE or OPE stimulation,  $177 \pm 8.4 \text{ nC}$ ,  $n = 127$ ), and virtual electrodes (i.e. CVE and IVE stimulation) created by triangular ( $174 \pm 6.2 \text{ nC}$ ,  $n = 122$ ) or hexagonal ( $193 \pm 9.1 \text{ nC}$ ,  $n = 84$ ) electrode shapes ( $p > 0.05$ , ANOVA on Ranks).

Spatial maps for an overlapping triangular and hexagonal electrode shape are shown in figure 4. In this example, the cortical response pattern to CPE stimulation was very similar to the repeat of CPE stimulation and the various

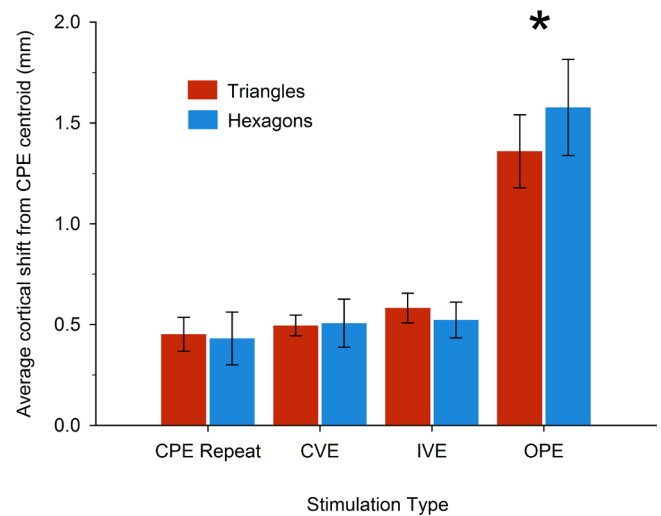


**Figure 5.** Bar chart showing the average distance between the centroid of activation calculated for stimulation of the CPE, and centroids calculated for every stimulation mode, including a repeat of CPE stimulation. Asterisk denotes group showing significant increase (RM ANOVA on Ranks,  $p < 0.001$ , Tukey post hoc test). No significant difference was observed between the average cortical shift of the repeat of the CPE and the two virtual electrode modes (CVE and IVE) ( $p > 0.05$ ). There was a significant shift between the centroids calculated for CPE stimulation and OPE stimulation ( $p < 0.001$ ). No significant differences were observed between triangular and hexagonal groups (RM ANOVA on Ranks,  $p > 0.05$ , Tukey post hoc test). Error bars show standard error of the mean.

virtual electrode stimulation configurations, but different to the OPE configuration. It should be noted that not all triangular and hexagonal electrode shapes shared a CPE or OPEs, therefore responses to each shapes were analysed separately. The average shift in cortical centroid location between the two repeats of CPE stimulation was found to be  $0.451 \pm 0.08 \text{ mm}$  and  $0.431 \pm 0.13$  for the 18 triangular and eight hexagonal shapes respectively (shown in figure 5). For both triangular and hexagonal shapes, centroid shift from CPE stimulation significantly depended on the stimulus configuration used (figure 5,  $p < 0.001$ , one-way RM ANOVA). Centroid shift between responses to CPE stimulation and CVE and IVE stimulation were not found to be

significantly different to the average shift between CPE repeats (figure 5,  $p > 0.05$ , Tukey post hoc). A significant shift in centroid location was observed between responses to CPE and OPE stimulation (figure 5,  $p < 0.001$ , Tukey post hoc). No significant difference was observed between the spread of cortical activity elicited by each stimulation mode ( $p > 0.05$ , one-way ANOVA, Dunn post hoc). No significant difference was observed in the spread of cortical activity between stimulation of single physical electrode stimulation ( $1/\tau = 1.84 \pm 0.17$ ,  $n = 58$ ) and virtual electrode stimulation of triangular ( $1/\tau = 2.06 \pm 0.17$ ,  $n = 57$ ) or hexagonal ( $1/\tau = 2.06 \pm 0.15$ ,  $n = 47$ ) electrode shapes. ( $p > 0.05$ , ANOVA on ranks).

### Predicting location of IVEs

To validate our method of predicting the angle of cortical centroid shift using retinotopy, we first attempted to predict the angle of shift between centroids calculated for responses to CPE and OPE stimulation, as the locations of physical electrodes in the eye can be directly determined from fundus imaging. Responses to CPE and OPE stimulation were recorded from 38 triangular and 19 hexagonal shapes. From these shapes, 41 unique CPE-OPE electrode pairs yielded thresholds. The difference between the expected and measured angles between CPE-OPE centroid pairs ( $\theta_{\text{error}}$ ) is plotted in a binned polar histogram (45° bin width) in figure 6. Statistical analysis showed that the distribution of  $\theta_{\text{error}}$  was not uniform ( $p < 0.01$ , Rayleigh's test), with a circular mean deviation from the predicted angle of  $-0.18^\circ$ .

In a similar manner, to determine whether we could predict the angle of centroid shift for responses to IVEs, shapes were included if a threshold could be calculated from at least one recording channel in response to CVE stimulation and at least one trial of IVE stimulation. CVE-IVE centroid pairs were excluded if the cortical centroid shift between them exceeded the mean average cortical distance between CPE and IVE centroids from the data shown in figure 5 by one standard error to rule out the effect of responses shifting to neighbouring cortical areas. Using these criteria, 41 triangular, 25 rectangular and 13 hexagonal shapes were included in analysis. Deviation from the predicted direction of centroid shift was calculated for 184 CVE-IVE pairs (103 from triangular, 19 from rectangular, and 62 from hexagonal shapes). Based on the analysis shown in figure 5, where repeated CPE and CVE stimulation resulted in a similar centroid shift, for this analysis we assumed that the peak of the electrical field produced from CVE stimulation would be located at the same point as the CPE for a given shape, and that the peak would shift in the direction of the physical electrode with the greater proportion of charge in the case of IVE stimulation with triangular or hexagonal shapes. For rectangular shapes, we expected the peak to shift toward the midpoint between the two electrodes that received the greater proportion of charge. An example of the method used to predict the angle of cortical centroid shift between a CVE-IVE pair of a hexagonal electrode shape is shown in figure 7.

Contrary to our expectations, for triangular shapes (shown in figure 8(a)), the  $\theta_{\text{error}}$  calculated for responses between

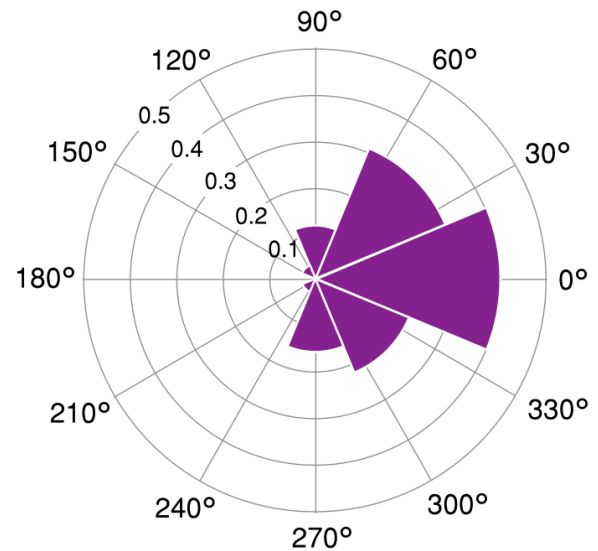


**Figure 6.** Polar probability density histogram showing the distribution of  $\theta_{\text{error}}$  calculated for 41 CPE-OPE pairs, grouped in to 45° bins. Binned values denote the difference between the predicted and measured direction of cortical centroid shift from CPE stimulation to OPE stimulation. The distribution was found to be non-uniform ( $p < 0.01$ , Rayleigh test). The circular mean for these values was  $-0.18^\circ$ . Radial axes show estimated probability density for each bin.

CVE and IVE stimulation were uniformly distributed with no preference in any direction ( $p > 0.05$ , Rayleigh's test). However, for rectangular and hexagonal shapes (shown in figures 8(b) and (c)), the distribution  $\theta_{\text{error}}$  were found to be non-uniform, with a circular mean deviation from the predicted angle of  $-13.41^\circ$  and  $-20.96^\circ$  respectively ( $p < 0.01$ , Rayleigh's test).

## Discussion

In this study, we investigated whether current steering could be extended to a 2D electrode array, allowing us to create virtual electrodes using more than two simultaneously stimulated electrodes. From our data, we have shown that we can reproduce certain spatial characteristics of cortical responses to stimulation of physical electrodes with virtual electrodes created by stimulation of up to six surrounding physical electrodes. While we were not able to create distinct IVEs when applying unequal stimulation weights, we did show that we could predict the direction of the shift in the centroid of cortical activity based on which electrodes received greater proportions of charge.

### Reproducing responses to physical electrodes with virtual electrodes

We found that equally-weighted simultaneous stimulation of electrodes in either triangular or hexagonal arrangements could elicit cortical responses with similar spatial characteristics to that of stimulation of the electrode in the centre of the shape. Confirming our initial hypothesis, the shift in centroid position between responses to CPE and CVE stimulation was



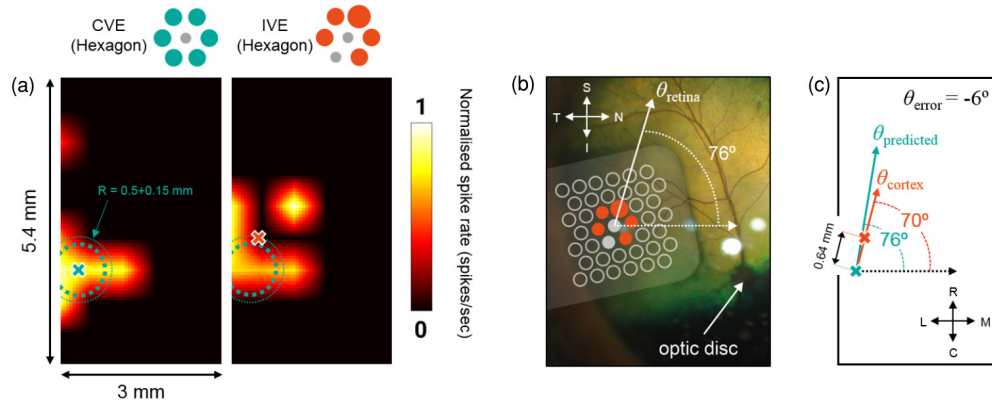


**Figure 7.** Diagrams showing example of centroid shift in the cortex and the methodology of directional prediction. (a) Two spatial maps showing patterns for CVE and IVE stimulation of the same hexagonal shape. The weighted centroids for each pattern are marked by the coloured X. The dotted circles show the mean (thicker line) and upper standard error (thinner line) of the average hexagonal IVE centroid shift from figure 5 (radius of  $0.5 \pm 0.15$  mm). (b) Fundus image with overlay of the stimulating array in its real position. Orange electrodes show the hexagon being stimulated in an IVE configuration. The solid white arrow shows the expected direction of shift of the electrical field peak from the peak of field produced by CVE stimulation at an angle of  $76^\circ$  from the horizontal which was used as the direction of the predicted centroid in the cortex. (c) Diagram comparing the measured direction between the centroids from spatial maps shown in (a), and the predicted direction based on retinal measurements. Note that the measured direction is within only  $6^\circ$  of the predicted direction.

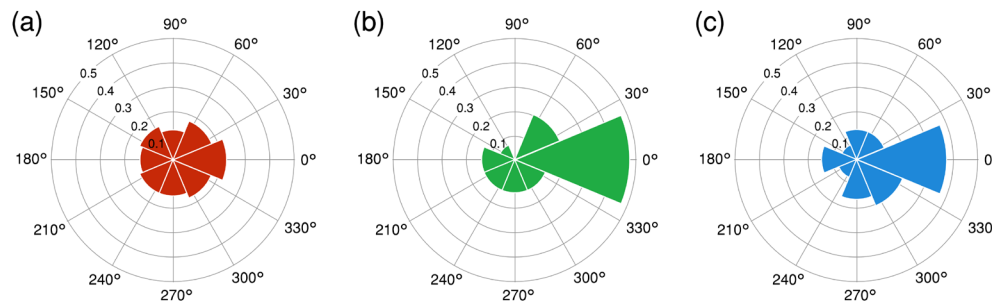


**Figure 8.** Polar probability density histogram showing the distribution of  $\theta_{\text{error}}$  calculated for CVE-IVE pairs, grouped in to  $45^\circ$  bins. (a)–(c) Show the differences between the predicted and measured direction of cortical centroid shift from CVE stimulation to IVE stimulation, for triangular ( $n = 103$ ), rectangular ( $n = 19$ ), and hexagonal ( $n = 63$ ) electrode shapes respectively. The distribution for (a) was found to be uniform ( $p > 0.05$ , Rayleigh test), however, (b) and (c) were found to be non-uniform ( $p < 0.01$ , Rayleigh test), with circular means of  $-13.41^\circ$  and  $-20.96^\circ$  respectively. Radial axes show estimated probability density for each bin.

no greater than the shift observed between repeats of CPE stimulation. Shift in cortical centroid position between CPE and OPE retinal stimulation, was significantly higher than between repeats of CPE stimulation. There was also no significant difference in the spread of neural activation elicited by physical electrode or virtual electrode stimulation. This indicates that CVE stimulation of these shapes created virtual electrodes in a similar location to the physical electrode in the centre of the shapes, producing responses with similar spatial characteristics (centroid and cortical spread measures) to CPE stimulation. This is consistent with our previous work with electrode pairs, which showed that cortical responses to physical and virtual retinal electrodes elicited similar levels of cortical activation spread, and that delivering equal proportions of charge to each electrode elicited responses with centroids approximately halfway between centroids calculated for each individual electrode [10]. Our results show that the ability to create virtual electrodes with cortical activation spread to physical electrodes is maintained with 2D current steering, and that the spatial linearity of field interactions remains consistent. Somewhat surprisingly, although we predicted IVE stimulation would elicit a centroid shift from CPE stimulation

greater than that of repeats of CPE stimulation, we found this was not the case. This data suggests IVE stimulation created a virtual electrode closer to the central electrode compared to the outer electrode receiving the greater charge proportion. Moreover, the thresholds found between CPE and CVE stimulation in total charge were similar, indicating a much reduced charge requirement on a per electrode basis when performing CVE stimulation. This indicates the CVE stimulation may be an attractive replacement for CPE stimulation when requiring low voltage stimulation, particularly for smaller sized electrodes where the impedances would be high.

### Creating IVEs

Due to the degree of variability in the centroid location calculated for responses to repeated CPE stimulation, it may have been that that virtual electrode produced when performing IVE stimulation did not shift the cortical response enough to be distinguished from this baseline noise, most likely due to an insufficient alteration to charge proportions. As such, we devised a method to determine whether there was a preferred shift toward the electrode/s with the greatest proportion of

charge. Our predictive technique is a very crude adaptation of Tusa's map of visual cortex and does not account for the curvature of the retinotopic map as it approaches the longitudinal fissure and the splenial sulcus [41, 42]. Our technique also relies on the assumption of the maintenance of similar scaling to the retina in all cortical directions.

To validate our technique, we first trialled it by calculating the directionality of the shift in centroids calculated for responses to CPE versus OPE stimulation. We showed that there was a statistical preference for the direction that we predicted, showing that this technique was a valid model. When applied to responses to CVE and IVE stimulation, we found that we also could predict the direction of cortical shift for rectangular and hexagonal shapes, using only the knowledge of which outer electrodes received greater proportions of charge. However this was not the case for triangular shapes. This may have been due to the differing geometry of electrode arrangements and proportions of charge between the shapes. Given our array of electrodes had a 1 mm pitch, and assuming absolute linearity in field interactions, the weighted shift in the centre of mass of the electric field in the retina for IVE stimulation for triangular, rectangular, and hexagonal electrode shapes would be 0.25 mm, 0.33 mm, and 0.33 mm respectively from the geometric centre. As there is a reduced shift for stimulation of triangular shapes, it may explain why we were unable to observe a measurable preference in the expected direction. However, while the theoretical basis for field shaping techniques such as current steering and focusing are predicated on the assumption of linear summation of field potentials, it does not necessarily imply a linear relationship between current weightings and the location of the peak of the summated electrical field. In the absence of a validated model of electrical stimulation from the suprachoroidal space, we cannot know for certain the effects of electrode arrangement on the shape of the resultant electric field.

The cortical centroids that did shift in the direction of the electrodes that received the greatest proportion of charge confirmed that IVE stimulation is shifting the electrical field in the retina, consistent with our previous work with electrode pairs [10]. However, the absence of significantly observable shifts in cortical centroids with IVE stimulation may also be a result of the generally broad spread of cortical activation elicited by monopolar stimulation. The large spread of the electrical potential in the retina [20, 43], coupled with undesired activation of axons of passage [44], may provide insufficient resolution to observe spatially discrete responses to IVEs. This is consistent with patient reports that phosphenes elicited through monopolar stimulation from the suprachoroidal space often appear large and overlap with phosphenes elicited by neighbouring physical electrodes [45]. Using a stimulating array that has smaller electrodes and is implanted closer to the target neurons, such as devices designed for epi- and sub-retinal placement, may result in more spatially discrete activation patterns. Using longer pulse widths (>25 ms) or sinusoidal stimulation has also shown promise in improving the selectivity of retinal neuron activation and avoiding activation of axons of passage. These techniques may result in more uniform and discrete cortical activation patterns and

phosphenes, and allow for more accurate centroid calculations [46, 47].

### *Implications and future directions*

This study demonstrates for the first time that virtual electrodes created by simultaneous stimulation of up to six physical electrodes can reproduce the spatial characteristics of responses to individual physical electrodes. These data also supports other studies that assert that field interactions are both predictable and repeatable, and, rather than a hindrance, have the potential to be a powerful tool in increasing the range of percepts that can be presented to patients.

Electrode failure is a significant issue for many prosthetic devices [23, 24]. Due to the complexity of making miniaturised and biocompatible devices, electrode arrays are fragile and prone to lead wire and electrode breakage. Due to the similarity between thresholds, centroid locations and spread of neural activation, it is possible that CPE stimulation and CVE stimulation of such geometric shapes will elicit similar percepts in patients. Using simultaneous stimulation of adjacent surrounding electrodes, the percept elicited by the failed electrode in the centre may be able to be replicated, compensating for the loss of sensory input. As it may take a significant amount of time and training for patients to be able to interpret the stimuli they are being presented with, the consistency of percepts elicited by a device will likely play a substantial role in its usefulness [48, 49]. Using virtual electrodes, device lifespan may be improved and will provide patients with longer-term consistent stimuli. Virtual electrodes may also replace the need for electrode-dense arrays, reducing manufacturing complexity. However, it may be prudent to include redundant physical electrodes available for virtual electrode stimulation in case of electrode failure. In a device with fewer electrodes, breakage of an electrode could have further reaching consequences on phosphene generation than a traditional electrode array, as a single electrode may be responsible for multiple percepts when used as part of different geometric shapes.

Incorporation of current steering in cochlear implant stimulation strategies have been shown to elicit additional pitch percepts [15], however the functional benefit to speech recognition has been minimal [17, 50]. This may in part be due to broad spread of current, resulting in perceptual overlap [51]. As mentioned earlier, psychophysical testing has shown that phosphenes often appear large and overlap with phosphenes elicited by neighbouring physical electrodes [45]. As such, creating additional phosphenes between these phosphenes would likely provide little functional benefit, as patients may have difficulty discriminating between them. In addition, phosphenes are typically elicited sequentially in order to reduce unwanted spatiotemporal electrical interactions [12, 13]. As timing between stimuli is compressed to accommodate greater numbers of phosphenes (those elicited by both physical electrodes and virtual electrodes), these interactions may become more prominent. Future-generation devices with improved electrode geometries and materials may be able to elicit more discrete discriminable phosphenes, however, for

present generation devices, current steering may need to be combined with a form of current focusing. Traditional forms of current focusing use local return configurations such as bipolar [39, 52], hexapolar [21, 39, 53], quasimonopolar [43, 54], and common ground stimulation [39]. These techniques may prove to be incompatible with this form of current steering as neighbouring return electrodes may need to be recruited to create virtual electrodes and so would be unavailable to act as current sinks. Focused multipolar (FMP) stimulation, which utilises simultaneous stimulation of surrounding electrodes with different weights and polarities to shape the electrical field, has been shown to yield a similar degree of reduction of spread of neural activation as hexapolar stimulation [20]. As the field is actively shaped by altering stimulation weights, it is possible that 2D steering could be incorporated in to the calculation of these weightings. Future studies should investigate the compatibility of these techniques and whether more discrete cortical patterns can be elicited using virtual electrodes.

### Limitations

We have used a number of measures such as centroid location, spread of neural activation, and cortical activation threshold in order to quantify the difference between the cortical responses to physical and virtual electrode stimulation. While these metrics show that virtual electrodes can reproduce certain properties of the cortical response, there are many other spatial and temporal components that we did not investigate that may impact on phosphene appearance. As such, we cannot claim with any certainty that phosphenes generated by physical or virtual electrode stimulation using surrounding electrodes would appear the same to patients. However, we believe that our measures still provide a strong argument that virtual electrodes created using 2D current steering can produce phosphenes in a similar location to those elicited by physical electrodes, and share a similar spread and perceptual threshold.

Further investigation should be conducted in to the limitations of this technique, such as the maximum physical distance between electrodes before electrical field interactions diminish. Due to time constraints, this study investigated only a limited number of current proportions. Experimenting with a wider range of unequal current weights may provide a more comprehensive understanding of the generation of IVEs. Delivery of different current amplitudes to electrodes simultaneously adds the engineering requirement of multiple independent current drives, increasing the technical complexity of the device. Multiple current drives may not be required to deliver equally-weighted stimulation, provided the impedance of the physical electrodes are similar. Stimulation of physical electrodes in irregular geometric arrangements may provide a more comprehensive way to produce virtual electrodes in regions other than the centre of a shape.

The cats used in this study were acutely-implanted and normally sighted. As such, there are a number of structural and functional differences between the visual system of these cats and visually-impaired patients. Firstly, there are many effects that occur following long-term implantation in patients, such

as chronic inflammation and fibrosis, that were not reflected in this study [55, 56]. Secondly, the morphology of a degenerated retina is very different to that of our normally-sighted cats. In addition to the loss of photoreceptors, there is also a significant degree of remodelling and indirect cell death that occurs in the inner layers of the retina [57]. There is also substantial attenuation of the retinal vasculature and thinning of the choroid in response to reduced metabolic demand [58, 59]. Due to loss of visual input there is also significant cortical remapping, however, recent studies have shown that prolonged use of retinal prostheses may partially reverse this [60]. While we would not expect retinal degeneration to affect the shape of the electrical fields produced by current steering, it is possible that the altered physiological conditions may result in unexpected cortical activity. Our previous work in a cat model of retinal degeneration has shown increased cortical thresholds, decreased cortical spread, and increased size of retinal receptive fields [61, 62]. While this may not affect the location of phosphenes elicited by virtual electrodes, shape, spread, and other spatio-temporal properties may be different in degenerated eyes. Future studies in long term implanted blind cats would provide a more representative insight in to the benefits of this technique.

### Conclusion

This study shows for the first time that virtual electrodes can be created using 2D current steering with simultaneous stimulation of up to six physical electrodes. Virtual electrodes created using this method produced cortical responses that shared similar thresholds, centroid locations and activation spread to responses elicited by the CPEs surrounded by the electrodes used for steering in the form of a geometric shape. We have also shown that virtual electrodes can be shifted in desired directions by altering the proportions of currents applied to steering electrode groups, however the change in charge proportions to observe this directionality preference needs to be large enough. This technique could provide a greater level of control over the location of phosphenes in patients' visual field, increase the number of percepts that can be presented to patients, as well as compensate for faulty physical electrodes. Further studies in long-term implanted blind feline models could give clearer insights in to the translational benefit of these techniques.

### Acknowledgments

The authors wish to thank Stephanie Epp, Ceara McGowan, Ali Almasi, Felix Aplin, Kerry Halupka, Faith Lamont, Rodney Millard, Alison Neil, Alexia Saunders, Evgeni Sergeev, Dimitra Stathopoulos, Patrick Thien, and Sam Titchener for assistance. Also, thanks to Penny Allen and Chi Luu for implanting the suprachoroidal device. Funding for this research was provided by the National Health and Medical Research Council (NHMRC) Project Grant #1063093 and the Bart Reardon PhD Scholarship. The Bionics Institute acknowledges the support it receives from the Victorian Government through its Operational Infrastructure Support Program.



## ORCID iDs

Thomas C Spencer  <https://orcid.org/0000-0002-2632-8405>

James B Fallon  <https://orcid.org/0000-0003-2686-3886>

Mohit N Shivdasani  <https://orcid.org/0000-0002-0692-4971>

## References

- [1] Shepherd R K, Shivdasani M N, Nayagam D A X, Williams C E and Blamey P J 2013 Visual prostheses for the blind *Trends Biotechnol.* **31** 562–71
- [2] Weiland J D, Liu W and Humayun M S 2005 Retinal prosthesis *Annu. Rev. Biomed. Eng.* **7** 361–401
- [3] Hartong D T, Berson E L and Dryja T P 2006 Retinitis pigmentosa *Lancet* **368** 1795–809
- [4] Ahuja A K, Dorn J D, Caspi A, McMahon M J, Dagnelie G, Dacruz L, Stanga P, Humayun M S and Greenberg R J 2011 Blind subjects implanted with the Argus II retinal prosthesis are able to improve performance in a spatial-motor task *Br. J. Ophthalmol.* **95** 539–43
- [5] Shivdasani M N, Sinclair N C, Dimitrov P N, Varsamidis M, Ayton L N, Luu C D, Perera T, McDermott H J and Blamey P J 2014 Factors affecting perceptual thresholds in a suprachoroidal retinal prosthesis *Investigative Ophthalmol. Vis. Sci.* **55** 6467–81
- [6] Ayton L N et al 2014 First-in-human trial of a novel suprachoroidal retinal prosthesis *PLoS One* **9** e115239
- [7] Wilke R et al 2011 Spatial resolution and perception of patterns mediated by a subretinal 16-electrode array in patients blinded by hereditary retinal dystrophies *Investigative Ophthalmol. Vis. Sci.* **52** 5995–6003
- [8] da Cruz L et al 2016 Five-year safety and performance results from the argus II retinal prosthesis system clinical trial *Ophthalmology* **123** 2248–54
- [9] Chaturvedi A, Foutz T J and McIntyre C C 2012 Current steering to activate targeted neural pathways during deep brain stimulation of the subthalamic region *Brain Stimul.* **5** 369–77
- [10] Dumm G, Fallon J B, Williams C E and Shivdasani M N 2014 Virtual electrodes by current steering in retinal prostheses *Investigative Ophthalmol. Vis. Sci.* **55** 8077–85
- [11] Luo X, Landsberger D M, Padilla M and Srinivasan A G 2010 Encoding pitch contours using current steering *J. Acoust. Soc. Am.* **128** 1215–23
- [12] Horsager A, Greenberg R J and Fine I 2010 Spatiotemporal interactions in retinal prosthesis subjects *Investigative Ophthalmol. Vis. Sci.* **51** 1223–33
- [13] Horsager A, Boynton G M, Greenberg R J and Fine I 2011 Temporal interactions during paired-electrode stimulation in two retinal prosthesis subjects *Investigative Ophthalmol. Vis. Sci.* **52** 549–57
- [14] Wilke R G H, Moghadam G K, Lovell N H, Suanning G J and Dokos S 2011 Electric crosstalk impairs spatial resolution of multi-electrode arrays in retinal implants *J. Neural Eng.* **8** 046016
- [15] Firszt J B, Koch D B, Downing M and Litvak L 2007 Current steering creates additional pitch percepts in adult cochlear implant recipients *Otol. Neurotol.* **28** 629–36
- [16] Koch D B, Downing M, Osberger M J and Litvak L 2007 Using current steering to increase spectral resolution in CII and HiRes 90 K users *Ear Hear.* **28** 38S–41S
- [17] Firszt J B, Holden L K, Reeder R M and Skinner M W 2009 Speech recognition in cochlear implant recipients: comparison of standard HiRes and HiRes 120 sound processing *Otol. Neurotol.* **30** 146–52
- [18] Barbe M T, Maarouf M, Alesch F and Timmermann L 2014 Multiple source current steering—a novel deep brain stimulation concept for customized programming in a Parkinson's disease patient *Park. Relat. Disord.* **20** 471–3
- [19] Martens H C F, Toader E, Decré M M J, Anderson D J, Vetter R, Kipke D R, Baker K B, Johnson M D and Vitek J L 2011 Spatial steering of deep brain stimulation volumes using a novel lead design *Clin. Neurophysiol.* **122** 558–66
- [20] Spencer T C, Fallon J B, Thien P C and Shivdasani M N 2016 Spatial restriction of neural activation using focused multipolar stimulation with a retinal prosthesis *Investigative Ophthalmol. Vis. Sci.* **57** 3181
- [21] Jepson L H, Hottowy P, Mathieson K, Gunning D E, Dąbrowski W, Litke A M and Chichilnisky E J 2014 Spatially patterned electrical stimulation to enhance resolution of retinal prostheses *J. Neurosci.* **34** 4871–81
- [22] Halupka K J, Shivdasani M N, Cloherty S L, Grayden D B, Wong Y T, Burkitt A N and Meffin H 2017 Prediction of cortical responses to simultaneous electrical stimulation of the retina *J. Neural Eng.* **14** 016006–22
- [23] Blomstedt P and Hariz M I 2005 Hardware-related complications of deep brain stimulation: a ten year experience *Acta Neurochir.* **147** 1061–4
- [24] Terasawa Y, Tashiro H, Nakano Y, Osawa K and Ozawa M 2013 Safety assessment of semichronic suprachoroidal electrical stimulation to rabbit retina *Conf. Proc. ... Annual Int. Conf. of the IEEE Engineering in Medicine and Biology Society* vol 2013 pp 3567–70
- [25] Cicione R, Fallon J B, Rathbone G D, Williams C E and Shivdasani M N 2014 Spatiotemporal interactions in the visual cortex following paired electrical stimulation of the retina *Investigative Ophthalmol. Vis. Sci.* **55** 7726–38
- [26] Villalobos J et al 2013 A wide-field suprachoroidal retinal prosthesis is stable and well tolerated following chronic implantation *Investigative Ophthalmol. Vis. Sci.* **54** 3751–62
- [27] Saunders A L et al 2014 Development of a surgical procedure for implantation of a prototype suprachoroidal retinal prosthesis *Clin. Exp. Ophthalmol.* **42** 665–74
- [28] John S E, Shivdasani M N, Leuenberger J, Fallon J B, Shepherd R K, Millard R E, Rathbone G D and Williams C E 2011 An automated system for rapid evaluation of high-density electrode arrays in neural prostheses *J. Neural Eng.* **8** 036011
- [29] Tassinari G, Bentivoglio M, Chen S and Campara D 1997 Overlapping ipsilateral and contralateral retinal projections to the lateral geniculate-nucleus and superior colliculus in the cat—a retrograde triple labeling study *Brain Res. Bull.* **43** 127–39
- [30] Payne B R 1994 Neuronal interactions in cat visual cortex mediated by the corpus callosum *Behav. Brain Res.* **64** 55–64
- [31] Wässle H and Illing R 1980 The retinal projection to the superior colliculus in the cat: a quantitative study with HRP *J. Comp. Neurol.* **190** 333–56
- [32] Illing R and Wässle H 1981 The retinal projection to the thalamus in the cat: a quantitative investigation and a comparison with the retinotectal pathway *J. Comp. Neurol.* **202** 265–85
- [33] Fallon J B, Irving S, Pannu S S, Tooker A C, Wise A K, Shepherd R K and Irvine D R F 2016 Second spatial derivative analysis of cortical surface potentials recorded in cat primary auditory cortex using thin film surface arrays: Comparisons with multi-unit data *J. Neurosci. Methods* **267** 14–20
- [34] Leung R T, Shivdasani M N, Nayagam D A X and Shepherd R K 2015 *In vivo* and *in vitro* comparison of the charge injection capacity of platinum macroelectrodes *IEEE Trans. Biomed. Eng.* **62** 849–57



- [35] Heffer L F and Fallon J B 2008 A novel stimulus artifact removal technique for high-rate electrical stimulation *J. Neurosci. Methods* **170** 277–84
- [36] Boinagrov D, Pangratz-Fuehrer S, Goetz G and Palanker D 2014 Selectivity of direct and network-mediated stimulation of the retinal ganglion cells with epi-, sub- and intraretinal electrodes *J. Neural Eng.* **11** 26008
- [37] Shivdasani M N, Luu C D, Cicione R, Fallon J B, Allen P J, Leuenberger J, Suaning G J, Lovell N H, Shepherd R K and Williams C E 2010 Evaluation of stimulus parameters and electrode geometry for an effective suprachoroidal retinal prosthesis *J. Neural Eng.* **7** 36008
- [38] Wong Y T, Chen S C, Kerdraon Y A, Allen P J, McCombe M F, Morley J W, Lovell N H and Suaning G J 2008 Efficacy of supra-choroidal, bipolar, electrical stimulation in a vision prosthesis *Annual Int. Conf. of the IEEE Engineering in Medicine and Biology Society* vol 2008 pp 1789–92
- [39] Cicione R, Shivdasani M N, Fallon J B, Luu C D, Allen P J, Rathbone G D, Shepherd R K and Williams C E 2012 Visual cortex responses to suprachoroidal electrical stimulation of the retina: effects of electrode return configuration *J. Neural Eng.* **9** 36009
- [40] Shivdasani M N, Fallon J B, Luu C D, Cicione R, Allen P J, Morley J W and Williams C E 2012 Visual cortex responses to single- and simultaneous multiple-electrode stimulation of the retina: implications for retinal prostheses *Investigative Ophthalmol. Vis. Sci.* **53** 6291–300
- [41] Tusa R 1978 The retinotopic organization of area 17 (striate cortex) in the cat *J. Comp. Neurol.* **177** 213–35
- [42] Tusa R J, Palmer L A, Rosenquist A C and Palmer L A 1979 Retinotopic organization of area 18 and 19 in the cat *J. Comp. Neurol.* **185** 213–36
- [43] Matteucci P B, Chen S C, Tsai D, Dodds C W D, Dokos S, Morley J W, Lovell N H and Suaning G J 2013 Current steering in retinal stimulation via a quasimonopolar stimulation paradigm *Investigative Ophthalmol. Vis. Sci.* **54** 4307–20
- [44] Schiefer M A and Grill W M 2006 Sites of neuronal excitation by epiretinal electrical stimulation *IEEE Trans. Neural Syst. Rehabil. Eng.* **14** 5–13
- [45] Sinclair N C, Shivdasani M N, Perera T, Gillespie L N, McDermott H J, Ayton L N and Blamey P J 2016 The appearance of phosphenes elicited using a suprachoroidal retinal prosthesis *Investigative Ophthalmol. Vis. Sci.* **57** 4948–61
- [46] Freeman D K, Eddington D K, Rizzo J F and Fried S I 2010 Selective activation of neuronal targets with sinusoidal electric stimulation *J. Neurophysiol.* **104** 2778–91
- [47] Weitz A C, Nanduri D, Behrend M R, Gonzalez-Calle A, Greenberg R J, Humayun M S, Chow R H and Weiland J D 2015 Improving the spatial resolution of epiretinal implants by increasing stimulus pulse duration *Sci. Transl. Med.* **7** 1–12
- [48] Dagnelie G 2008 Psychophysical evaluation for visual prosthesis *Annu. Rev. Biomed. Eng.* **10** 339–68
- [49] Geruschat D R and Deremeik J 2011 Activities of daily living and rehabilitation with prosthetic vision *Visual Prosthetics* (Berlin: Springer) pp 413–24
- [50] Buechner A, Brendel M, Krüeger B, Frohne-Büchner C, Nogueira W, Edler B and Lenarz T 2008 Current steering and results from novel speech coding strategies *Otol. Neurotol.* **29** 203–7
- [51] George S S, Shivdasani M N, Wise A K, Shepherd R K and Fallon J B 2015 Electrophysiological channel interactions using focused multipolar stimulation for cochlear implants *J. Neural Eng.* **12** 66005
- [52] Gerhardt M, Groeger G and Maccarthy N 2011 Monopolar versus bipolar subretinal stimulation—an *in vitro* study *J. Neurosci. Methods* **199** 26–34
- [53] Habib A G, Cameron M A, Suaning G J, Lovell N H and Morley J W 2013 Spatially restricted electrical activation of retinal ganglion cells in the rabbit retina by hexapolar electrode return configuration *J. Neural Eng.* **10** 36013
- [54] Khalili Moghaddam G, Lovell N H, Wilke R G H, Suaning G J and Dokos S 2014 Performance optimization of current focusing and virtual electrode strategies in retinal implants *Comput. Methods Programs Biomed.* **117** 334–42
- [55] Nayagam D A X et al 2014 Chronic electrical stimulation with a suprachoroidal retinal prosthesis: a preclinical safety and efficacy study *PLoS One* **9** e97182
- [56] Roessler G et al 2009 Implantation and explantation of a wireless epiretinal retina implant device: observations during the EPIRET3 prospective clinical trial *Investigative Ophthalmol. Vis. Sci.* **50** 3003–8
- [57] Fariss R N, Li Z Y and Milam A H 2000 Abnormalities in rod photoreceptors, amacrine cells, and horizontal cells in human retinas with retinitis pigmentosa *Am. J. Ophthalmol.* **129** 215–23
- [58] Grunwald J E, Maguire A M and Dupont J 1996 Retinal hemodynamics in retinitis pigmentosa *Am. J. Ophthalmol.* **122** 502–8
- [59] Dhoot D S, Huo S, Yuan A, Xu D, Srivistava S, Ehlers J P, Traboulsi E and Kaiser P K 2013 Evaluation of choroidal thickness in retinitis pigmentosa using enhanced depth imaging optical coherence tomography *Br. J. Ophthalmol.* **97** 66–9
- [60] Humayun M S 2017 Argus II clinical trial update *Annual Meeting of the Association for Research in Vision and Ophthalmology*
- [61] Halupka K J et al 2017 Neural responses to multielectrode stimulation of healthy and degenerate retina *Investigative Ophthalmol. Vis. Sci.* **58** 3770
- [62] Aplin F P, Fletcher E L, Luu C D, Vessey K A, Allen P J, Guymer R H, Shepherd R K and Shivdasani M N 2016 Stimulation of a suprachoroidal retinal prosthesis drives cortical responses in a feline model of retinal degeneration *Investigative Ophthalmol. Vis. Sci.* **57** 5216–29